Conf-9505146--1

SAND94-2965C

FINITE-ELEMENT ANALYSES OF BLADE AND SLOT COATING FLOWS USING AN IMPLICIT PSEUDO-SOLID DOMAIN MAPPING TECHNIQUE COUPLED WITH UNSTRUCTURED GRIDS

K. S. Chen, P. R. Schunk and P. A. Sackinger

Organization 1511
Manufacturing & Environmental Fluid Dynamics Dept.
Sandia National Laboratories
Albuquerque, New Mexico 87185–0827

December 4, 1994

*This work was performed at Sandia National Laboratories for the U. S. Department of Energy under contract number DE-AC04-94AL85000.

†Draft manuscript for the TAPPI Third Coating Fundamentals Symposium

Abstract

In coating processes (e.g. in blade coating) the flow domain inherently contains free surfaces and three-phase contact lines, and characteristic length scales of flow features in the dimension transverse to the web-movement vary by an order of magnitude or more (from a fraction of a millimeter or more to tens of microns or less). The presence of free surfaces and three-phase contact lines, and the sudden changes of flow geometry and directions create difficulties in theoretical analyses of such flows. Though simulations of coating flows via finite-element methods using structured grids have been reportedly demonstrated in the literature, achieving high efficiency of such numerical experiments remains a grand challenge - mainly due to difficulties in local mesh-refinement and in avoiding unacceptably distorted grids. High efficiency of computing steady flow fields under various process conditions is crucial in shortening turn-around time in design and optimization of coating-flow processes. In this paper we employ a fully-implicit, pseudo-solid, domain mapping technique coupled with unstructured meshes to analyze blade and slot coating flows using Galerkin's method with finite element basis functions. We demonstrate the robustness and efficiency of our unique technique in circumventing shortcomings of mesh-motion schemes currently being used in the coating-flow research community. Our goal is to develop an efficient numerical tool, together with a suitable optimization toolkit, that can be used routinely in design and optimization of coating-flow processes.

1 Introduction

To remain competitive and profitable in the coating industry one needs to minimize turn-around times for process design and optimization and to operate processes within proper "coating windows" that help ensure success in meeting the highest product-quality specifications and the lowest possible production costs. In recent years advances in numerical analyses of coating flows and computer hardware have made it possible to conduct numerical coating-flow experiments on workstations (and of course Cray-like supercomputers), though mainly for process understanding. To fully realize the impact of numerical simulations on the 'bottom line' of the coating industry, however, we need to go beyond the stage of process understanding and march into that of process design and optimization. Indeed, computer simulation (e.g. via finite-element analysis) can be an important tool in process design and optimization and in mapping out "coating windows". The reason for this is simple – once a validated and calibrated computer model is developed, it is much less time-consuming and much more cost-effective to conduct process design and optimization using a computer workstation than to execute an exhaustive set of experiments in a pilot-plant coating facility. Of course, key experiments will still have to be performed in a coater to benchmark the computer simulation to actual coating experiments; but fewer such experiments will be needed when process design and optimization are first made using a computer. Specifically, we are motivated by the industry's common need and goal to develop an efficient, finite-element analysis code, along with a suitable optimization tool kit, that can be used for routine process design and optimization.

In most (if not all) liquid coating-flow processes (e.g. in blade coating) the flow domain inherently contains free surfaces and three-phase contact lines, and the characteristic length scales of flow features in the dimension transverse to the web-movement vary by an order of magnitude or more (from a fraction of a millimeter or more to tens of microns or less). The presence of free surfaces and three-phase contact lines, and the sudden changes of flow geometry and directions create difficulties in theoretical analyses of such flows. Though simulations of coating flows such as blade coating via finite-element methods using structured grids have been reportedly demonstrated in the literature (e.g. Kistler and Scriven 1983, Christodoulou and Scriven 1992, Pranckh and Scriven 1988, Schunk 1989, Sartor 1990, Chen 1992, Benjamin 1994), achieving high efficiency of such numerical experiments remains a grand challenge – mainly due to difficulties in performing the local mesh refinement needed to capture important features of flow fields that have disparate length scales, and in avoiding unacceptably distorted grids. In fact, due to low efficiency and cumbersome user input in the simulation process, no extensive parameter study on blade coating flow has been reported in the open literature. High efficiency of computing steady, incompressible, viscous flow fields under various process conditions is crucial in shortening turn-around time in design and optimization of coating-flow processes. The key to achieving high efficiency in finite-element analyses of coating flows lies in the ability to:

1. fully couple the computation of flow-field variables with that of mesh-motion;
2. properly move grids to follow flow-domain shape in a way that minimizes mesh distor-

tions;

3. locally refine finite-element mesh where complex flow physics (e.g. flows near three-phase contact lines and in regions with sudden changes in flow geometry and directions) are present;

4. significantly reduce and simplify user input to the simulation process;

5. easily start up the simulation process (i.e. readily compute predictions of a new coating flow configuration).

An unstructured grid makes it possible to achieve local mesh refinement (in regions where complex flows occur) without having to add unnecessary unknowns to regions where flow physics are simple; this translates to saving computational costs and shortening turn-around process development time. In two-dimensional finite-element analysis using quadrilateral elements, an unstructured grid allows irregular element connectivity – an interior node can be shared by four, or fewer than four or more than four neighboring elements; in contrast, a structured grid generates regular element connectivity – each interior node is uniformly shared by four neighboring elements. The ability to refine a mesh locally is particularly important in process design and optimization studies and in "coating windows" mapping, in which a multi-dimensional parameter space needs to be explored to arrive at the optimal design or to determine the most robust "ranges" of operation. In these studies, locations and sizes of complex-flow regions vary in response to changes in process parameters.

In this paper we employ a fully-implicit, pseudo-solid, domain mapping technique coupled with unstructured meshes to analyze blade and slot coating flows using Galerkin's method with finite element basis functions. The word "fully-implicit" refers to the full coupling of the computation of flow-field variables with that of grid motion or position; that is, nodal unknowns of velocity components, pressure and grid-point coordinates are solved simultaneously using a Newton-Raphson iteration in order to achieve rapid convergence within a few iterations. By pseudo-solid, we mean to treat the finite-element mesh as if it were embedded in a solid continuum phase that extends over the computational domain for the free boundary problem. The mechanical properties of the pseudo-solid continuum are chosen entirely for the convenience of the mesh and have no inherent physical significance to the coating flow; a simple, linear-elastic, solid continuum described by a Young's modulus and a Poisson's ratio completely govern the internal deformations of the finite element mesh. Domain mapping implies that every nodal position in the mesh is mapped from an (educated) initial guess of the flow domain (including free surfaces) to the actual flow domain obtained from solving the flow and mesh deformation equations; this means that there is a nodal-position displacement unknown associated with each node within the domain (not just those along the free surfaces and interfaces). Using prototypical blade- and slot-coating flows as examples, we demonstrate the robustness and efficiency of our unique technique in circumventing shortcomings of mesh deformation schemes currently being used in the coating-flow research community. We chose blade and slot coating flows as test examples in our present study because of their wide-spread application in the paper-coating industry. Work reported in

the present paper reflects only the beginning of our research efforts at Sandia National Laboratories, which aim at developing a comprehensive software package to be used in routine design and optimization of coating-flow processes.

2 Model Formulation and Technical Approach

In this section we lay out the essential principles that govern motion or deformation of the finite-element mesh, coating-liquid flows, and substrate deformation. Since our focus is on the demonstration of robustness and efficiency of our novel mesh-deformation algorithm in analyzing blade and slot coating flows, the present study is restricted to isothermal flows of Newtonian liquids. Moreover, we consider a deformable, but impermeable, substrate and a rigid blade. Blade deflection/bending due to hydrodynamic-pressure loading and liquid penetration into substrate due to capillary action and hydrodynamic-pressure forcing will be taken into account in future studies. Also, effects of non-Newtonian rheology (e.g. shear thinning) will be presented elsewhere.

2.1 Initial Mesh Generation

We use FASTQ, an interactive two-dimensional finite-element mesh generation computer program developed at Sandia National Laboratories (T. D. Blacker 1988), to discretize the initial flow domain, which generates unstructured grids of quadrilateral elements (structured grids can also be generated when so desired). FASTQ employs a "paving" or "tiling" algorithm to discretize arbitrary geometries without causing undesirable mesh distortions. It also employs a set of "higher-order" primitives which have been developed for automatic meshing of commonly encountered shapes such as triangles, a semi-circles, etc.

2.2 Mesh Motion or Deformation

Details regarding the basic concepts, underlying assumptions, mathematical development and validity of the fully-implicit, pseudo-solid, domain mapping technique have been reported elsewhere (Sackinger, Schunk and Rao 1994). Accordingly, only the essence of this technique is provided here. Fundamentally, the fully-implicit, pseudo-solid mesh deformation algorithm relies on the concept of a pseudo-solid material that fills some given initial geometry of a computational domain. This initial computational domain may be discretized using any finite element mesh generator (e.g., FASTQ); the primary mission of the mesh generator is to produce a structured or unstructured grid of elements that are nearly uniform in size and without severe angles. Using the mesh deformation algorithm, these elements will undergo deformation as particles of a linear elastic solid according to whatever necessary displacements are required to bring the shape of the computational domain into compliance with the free boundary problem posed by the coating flow physics.

Given an initial guess of the domain shape, suppose that the particles of the pseudo-solid material in this geometry are specified as a function of spatial coordinates as

$$\mathbf{X}_{\text{initial}} = \mathbf{x}, \qquad \mathbf{x} \in \mathcal{D}_{\text{initial}}, \tag{1}$$

as shown in Figure 1. This initial configuration of the pseudo-solid is assumed to be given and to be topologically similar to the final deformed configuration. The fixed initial configuration of the pseudo-solid is referenced repeatedly during the course of the Newton iteration (for solving the nonlinear flow-field and mesh-motion equations) because a mapping of the initial configuration to a specific final deformed configuration is sought. Thus, the *mapping* to the final configuration depends on both the initial configuration and the final configuration.

As a consequence of the flow-field equations and the distinguishing boundary conditions (e.g. the kinematic/stress condition along free surfaces and the force-balance condition along the interface between coating liquid and the deformable substrate surface), the solution of the free boundary problem will include the required displacement to map $\mathcal{D}_{\text{initial}}$ to $\mathcal{D}_{\text{final}}$ so that

$$\mathbf{X}_{\text{final}} = \mathbf{x}, \qquad \mathbf{x} \in \mathcal{D}_{\text{final}}, \tag{2}$$

where $\mathbf{X}_{\text{final}}$ is as defined in Figure 1.

A simple displacement mapping based on the concept of a deforming pseudo-solid continuum is chosen here to describe the mapping between the initial and final domain, i.e.,

$$\mathbf{x} = \mathbf{X}_{\text{initial}} + \mathbf{d}(\mathbf{x}), \tag{3}$$

so that the mapping from the initial configuration to a deformed configuration is described by a single displacement vector $\mathbf{d}(\mathbf{x})$. The locations of all of the boundaries of the domain undergo this same displacement mapping,

$$\mathbf{x} = \mathbf{X}_{\text{initial}} + \mathbf{d}(\mathbf{x}), \qquad \mathbf{x} \in \partial\mathcal{D}. \tag{4}$$

Here, the idea for the displacement mapping is taken directly from continuum mechanics of deformable media. Each material point of the deformed pseudo-solid computational domain may be identified with a material point in the initial configuration of the domain; the Lagrangian description of the pseudo-solid describes the motion of the finite elements spanning the coating flow domain. The objective is to determine the unknown displacement field $\mathbf{d}(\mathbf{x})$ that provides a consistent solution to the free boundary problem. The displacement $\mathbf{d}$ is a continuous function of position that provides a one-to-one mapping between different configurations of the pseudo-solid, including the configuration that is consistent with the overall solution of a coating flow problem.

The differential equations that govern the internal mesh deformation are those of static equilibrium of a linear elastic solid with no internal body forces. Thus,

$$0 = \nabla \cdot \mathbf{S} \tag{5}$$

with,

$$\mathbf{S} = \lambda \text{tr}(\mathbf{E})\mathbf{I} + 2\mu\mathbf{E}, \tag{6}$$

where λ and μ are Lamé coefficients, $\mathbf{I}$ is the identity tensor, and $\mathbf{E}$ is the strain tensor,

$$\mathbf{E} = \frac{1}{2}\left[\nabla \mathbf{d} + \nabla \mathbf{d}^{\dagger}\right], \tag{7}$$

using the spatial gradients of the displacement, $\mathbf{d}$. These equations are used to determine the required internal displacements of the mesh.

In addition to the bulk equations governing the internal motion of the mesh, the pseudo-solid displacement mapping relies on *distinguishing conditions* (DCs) for enforcing the relevant physics of free boundaries on the pseudo-solid. Using this technique, all boundaries of the computational domain are, in principle, free to deform. In many cases, however, the boundaries of the flow domain do not distort to any appreciable extent and may be regarded as fixed in space and described in simple geometric terms; this would include stiff solid surfaces such as blades, slot-die faces, and rigid substrates. Other boundaries, such as fluid/air interfaces or interfaces between the fluid and a deformable substrate, may deform according to the physics governing the balances of material and momentum at the interface and are greatly affected by the flow conditions.

The rigid surfaces are conveniently described as level sets of surfaces in three dimensions or curves in two dimensions; straight lines and planes are described as

$$ax + by + cz + d = 0, \tag{8}$$

where $c = 0$ for two dimensional plane regions separated by a straight line. Such specification of nominally fixed boundaries is helpful in the formulation of a coating flow problem, since it permits the user to exercise greater control over the geometry of the domain. This is useful in the context of determining desirable operating and design parameters that are influenced by the geometry of rigid surfaces in the coater, where parameter studies are needed.

Equation 8 and the equations developed below as noted, are used as distinguishing conditions in the pseudo-solid mesh deformation algorithm. In essence, the constraint acts like a very strong potential well in the normal direction, insofar as the pseudo-solid is concerned.

As for free surfaces, additional distinguishing conditions are derived from force balance and material continuity requirements (e.g. kinematic condition) to locate their positions; it is in these distinguishing conditions that the flow field and the mesh motion equations are closely coupled. There are a variety of important DCs that arise in the analysis of coating flows and these are described in the next section.

2.3 Coating Flows

Steady flow of liquid is governed by the Cauchy equation of momentum conservation and the continuity equation of mass conservation:

$$\rho \mathbf{v} \cdot \nabla \mathbf{v} = \nabla \cdot \mathbf{T} + \rho \mathbf{g}, \tag{9}$$

$$\nabla \cdot \mathbf{v} = 0. \tag{10}$$

where ρ is the coating-liquid density, $\mathbf{v}$ is the liquid velocity with respect to fixed spatial coordinates, $\mathbf{T}$ is the local total Cauchy stress of the flowing liquid, and $\mathbf{g}$ is the gravitational body force. For a Newtonian liquid, the local stress state, $\mathbf{T}$, is related to the local hydrodynamic pressure, p, and strain rate by

$$\mathbf{T} = -p\mathbf{I} + \mu\left[\nabla\mathbf{v} + (\nabla\mathbf{v})^{\dagger}\right], \tag{11}$$

where superscript † indicates the transpose operator. For a non-Newtonian (e.g. shear thinning) liquid, the above Newtonian constitutive relation can be replaced by a Carreau or Carreau-like model; however, such non-Newtonian effects are outside the scope of the present study.

In two dimensions, the traction boundary condition along the free surfaces is the force balance

$$\mathbf{n} \cdot \mathbf{T} = \sigma\frac{d\mathbf{t}}{ds} + p_a\mathbf{n}, \tag{12}$$

where $\mathbf{t}$ and $\mathbf{n}$, respectively, are the unit vectors tangent and normal to the free surface; σ is the liquid equilibrium surface tension; p_a is the pressure of the surrounding air, usually the ambient pressure. When vaccum is applied at the air/liquid interface (as is normally done at the upstream free surface in slot coating), p_a in the above equation needs to be replaced by p_b, pressure in the vacuum chamber. The other boundary condition of no mass transferred across a free surface is expressed by the kinematic condition:

$$\mathbf{n} \cdot \mathbf{v} = 0. \tag{13}$$

Along rigid, solid surfaces such as blade surfaces, slot-die faces, and undeformable substrate surfaces, no-slip and impenetrability call for a vanishing velocity, i.e. $\mathbf{v} = \mathbf{0}$. The same requirements at the substrate surface result in $\mathbf{v} = \mathbf{v}_w$ with $\mathbf{v}_w$ being the substrate or web velocity. In the vicinity of the apparent dynamic wetting line (i.e. where the upstream free surface meets the web as in a slot coating flow), the stress singularity of single-phase flow theory is alleviated by applying Navier's slip hypothesis:

$$\frac{1}{\beta}\mathbf{t}_w \cdot (\mathbf{v} - \mathbf{v}_w) = \mathbf{t}_w\mathbf{n}_w : \mathbf{T}. \tag{14}$$

Here β is the slip coefficient ($\beta \to 0$ corresponds to the no-slip conditions, while $\beta \to \infty$ corresponds to a shear-free boundary condition); $\mathbf{t}_w$ and $\mathbf{n}_w$ are, respectively, the unit vectors tangent and normal to the web surface. The angle of contact between the free surface and the web surface is the second boundary condition required by single-phase flow theory at the apparent wetting line:

$$\mathbf{n}_w \cdot \mathbf{n} = cos\theta_d. \tag{15}$$

Here, β and θ_d are to be regarded as empirical parameters, though θ_d can be drawn from experimentally determined correlations (see, e.g. Kistler 1992 and Chen 1992).

At the inflow boundaries, a plug-flow velocity profile is imposed for blade coating (a valid approximation if the inflow boundary is placed far enough upstream) and a fully-developed

channel-flow is assumed for slot coating. Moreover, the inflow-layer thickness is known and held fixed for blade coating. At the outflow boundary, i.e. somewhere far downstream on the web, flow is taken to be traction free and slope of the free surface is specified:

$$\mathbf{n} \cdot \mathbf{T} = 0, \qquad t = t_w. \tag{16}$$

For fully-developed flow, the slope of the free surface will be taken such that it is perpendicular to the outflow plane and parallel to the streamwise direction.

The substrate in our blade-coating study is taken to be a compressible sheet; it is deformable only perpendicular to its surface, its local compression being proportional to the local normal loading. In other words, we treat the deformable substrate as consisting of a series of "springs" that are parallel to each other. With this simplified treatment, nonlinear compressibility, nonlocal effects of normal loading, and deformation caused by tangential loading are neglected. This approximation has also been employed by Taylor (1978), and recently by Pranckh & Scriven (1988) and Chen & Scriven (1989) in similar applications. Thickness of the deformed substrate, H, is then given by

$$\mathbf{n}_w \mathbf{n}_w : \mathbf{T} = E(1 - \frac{H}{H_o}), \tag{17}$$

where $\mathbf{T}$ is the local total liquid stress at the substrate surface, H_o is the undeformed substrate thickness, and E is a proportional constant of substrate compression, which can be considered as the Young's modulus of the deformable substrate (or E/H_o as the spring constant).

2.4 Method of Solution

The discretized set of equations that govern liquid flow, substrate deformation and mesh motion are solved simultaneously using Galerkin's method with finite basis functions and Newton's method. An excellent account of the details involved in the general solution procedure has been provided by Sackinger, Schunk and Rao (1994) and thus only a brief description of the solution method is given below. We employed quadratic polynomial basis functions for velocity and coordinate displacement variables and piecewise linear ones for pressure. We applied Galerkin's method of weighted residuals to reduce the set of governing partial differential equations to a set of nonlinear algebraic equations for the nodal unknowns of velocity, pressure, and mesh displacement. The nonlinear algebraic residual equations are solved using Newton's method (i.e. they are linearized successively and a linear system of algebraic equations are solved at each iteration). We solved the matrix equations using a direct matrix solver with a sparse-storage format. The above solution procedure was carried out using GOMA, a computer code developed at Sandia National Laboratories, which specializes in simulations of coating flows and subsequent drying/solidification processes. GOMA is capable of simulating multiple physics – fluid flow, heat and mass transfer, chemical reaction and liquid/solid interaction (with solid mechanics).

The resultant number of unknowns in the matrix equations, $Ax = b$, system ranges from 7,000 to 9,000. All calculations were performed using a SUN SPARCstation 20 workstation.

The first iteration took 15 to 20 minutes of CPU time, with considerable computational effort being expended on determining an optimal re-ordering of the equations to minimize matrix fill-in during the elimination process (recall, that for unstructured meshes, the matrix graph structure is also unstructured). Subsequent iterations took only 10 to 15 minutes, since the matrix re-ordering map could be re-used. Parameter increment was so controlled that it usually took six iterations to converge to a steady state solution with a residual norm of less than 10^{-6}.

3 Results and Discussion

To demonstrate the robustness and efficiency of our mesh deformation technique coupled with unstructured grids in analyzing blade and slot coating flows, illustrative results are presented below.

3.1 Blade Coating Flow

Figure 2 schematically shows the governing principles and associated boundary conditions for the blade coating-flow process. To focus on how to analyze blade coating flows efficiently for the purpose of design and optimization, we have limited our present study to rigid blades but the substrate was allowed to deform unidirectionally (blade deflection/bending will be taken into account in future studies). Figure 3a shows a typical unstructured finite element mesh used in our blade coating-flow study. A structured grid (with two subregions) with about the same mesh resolution is presented in Figure 3b for comparison. As shown, the mesh is locally refined where needed (i.e. where complex flows occur) in the unstructured grid whereas the structured grid allows no such flexibility. As a result, the structured grid produces about 47% more total unknowns (12956 vs. 8818) than the unstructured grid. Consequently, the CPU time requirement when using the structured grid was nearly doubled (192%) compared with that when using the unstructured grid (for computing a steady flow field with fixed boundaries from a zero initial guess, which took 3 iterations to converge, the structured grid spent 103.1 minutes whereas it took only 53.6 minutes with the unstructured grid). Plainly, employing unstructured meshes achieved higher computational efficiency and thus lower costs. Another important point is that a structured grid (e.g. the one shown in Figure 3b) can result in severe mesh distortion (e.g. the angles approach 180°) as geometry is altered (e.g. when the blade installation angle approaches 90°, i.e. vertical blade orientation) whereas an unstructured mesh (e.g. the one shown in Figure 3a) preserves its integrity. It should be pointed out that a series of meshes have been explored with respect to solution accuracy (measured by the degree of conservation of mass within each element, which can be visibly reflected in streamlines that are calculated by integration within each element throughout the entire mesh) before arriving at the meshes used in the present study.

A big challenge in coating flow analyses is 'startup' – that is, given a coating configuration (e.g. blade geometry and orientation) and process conditions, how can we compute the very

first flow field from which parameter continuation can be carried out? Indeed, a systematic strategy of analysis 'startup' is needed to ensure successful and efficient computation of the very first flow field. After some experimentation, we found an optimal startup sequence as presented in Figure 4, which was based on the realization that a free surface is shear-free (i.e. it can not support any shear stress). We first computed a steady flow field using fixed but slippery free surfaces: 1) The downstream free surface was taken to be flat and oriented parallel to the horizontal (x-axis) axis. 2) Along the downstream free surface, the velocity component normal to the free surface (i.e. the y-component velocity) was set to zero and the velocity component tangential to the surface surface (i.e. the x-component velocity) was computed using the vanishing shear-stress condition. 3) The upstream free surface was divided into three segments as shown in Figure 4 — the segment associated with the substrate was made parallel to the horizontal or x- axis and its velocity condition was imposed in the same way as that for the downstream free surface; the segment associated with the blade was oriented parallel to the vertical or y- axis, and along it the normal velocity component was set to zero and the tangential component was determined by the vanishing shear-stress condition; the two segments were connected by a-quarter-of-a-circle arch, along which velocity vector was required to be tangential to the surface. 5) The substrate surface was taken to be rigid and flat and along it the web velocity was imposed. Once a steady flow field solution for the fixed but slippery free surfaces was obtained, the downstream free surface was then set free (that is, the kinematic and normal-stress-balance conditions were applied) in order to locate the downstream-free-surface position. The upstream-free-surface position was similarly determined and finally we obtained a flow field with the downstream and upstream free surfaces. Desired steady flow states were then computed via parameter continuation.

Some typical results (velocity vector field, streamlines and pressure contours in the vicinity of the blade tip) for a steady blade coating flow are displayed in Figure 5. Enlargements of the gap region are also inserted for closer examination. Here, the incoming-layer thickness (h_{IN}) is 1.5 mm; web speed (U_W) 1 m/s; liquid density (ρ) 1000 kg/m^3; viscosity (μ) 50 $mPa \cdot s$; surface tension (σ) 50 mN/m; Young's modulus of substrate (E) 5 kPa; undeformed substrate thickness (H_o) 0.3 mm; blade installation/working angle (ϕ) 70°. For the conditions chosen, about 75% of the incoming coating liquid is metered by the blade as excess. As liquid travels toward the gap region, pressure rises; a pressure plateau is seen before it achieves its maximum just before the leading edge or the entrance of the gap (formed between the blade face and the substrate). As liquid is carried through the gap by the fast-moving web, pressure levels and takes a dip near the static separation line (pressure there actually becomes subambient) before returning to its ambient value. In response to mainly the hydrodynamic pressure force, the substrate deforms, though only slighly under the chosen conditions. As expected, the location of maximum deformation is seen to correspond to that of maximum pressure.

The robustness of our pseudo-solid mesh deformation technique is demonstrated in Figure 6. Figure 6a shows the deformed mesh sequence and Figure 6b displays the computed streamline sequence. In this illustration, blade installation/working angle (ϕ) was varied from 90° to 40° with the same mesh design or topology. Indeed, the upstream free-surface

shape underwent rather dramatic change and the mesh suffered quite large deformation. What is more, the entire sequence required only one small input from the analyst — the three coefficients that define the blade surface, which is a function of the blade installation/working angle and can be automated easily with a command script. In this sequence of continuation in blade installation/working angle, the liquid inertia effect has been neglected (i.e. the Reynolds number was set to zero). Also, the Young's modulus of the substrate sheet has been set high enough that the substrate would not deform.

Another demonstration of the robustness of our pseudo-solid mesh deformation technique is displayed in Figure 7. Here, liquid inertia effects were included in the flow-field computations and the blade installation/working angle was again varied from 90^o to 40^o. As shown, momentum impact helps thin the liquid layer near the blade tip and the upstream free surface moves inward toward the blade-face/substrate gap. Again, a mesh with the same topology was employed to compute the flow field in the sequence as shown in Figure 7a. Clearly, the mesh underwent huge deformation from the initial state to the last one in the sequence. Figure 7b details the hydrodynamic pressure response to varying the blade angle — peak or maximum pressure drops and the size of the pressure plateau region enlarges as the blade angle is reduced.

Lastly, Figure 8 shows the effect of varying blade-face angle (and also the bevel angle) on the flow field (velocity vector field in Figure 8a and pressure contour in Figure 8b). It is informative that creating a converging blade-face/substrate gap (i.e. when the blade rides on the toe) helps reduce peak pressure (and thus reduce substrate deformation) whereas a diverging gap (i.e when the blade rides on the heel) results in a higher peak pressure (and thus causes greater substrate deformation). More importantly, a diverging gap (or blade riding on the heel) produces a subambient-pressure zone (and also higher negative pressure) that can potentially result in coating-liquid cavitation and thus cause coating defects.

3.2 Slot Coating Flow

Figure 9 schematically shows the governing principles and associated boundary conditions for the slot coating-flow process. Here, we treat the substrate as undeformable as is often the case in actual applications. Figure 10a displays a typical unstructured mesh employed in our study. A structured mesh used by Sartor (1990) in his Ph.D. thesis study is shown in Figure 10b for comparison. Plainly, as shown in Figure 10, the unstructured grid offers flexibility of convenient local mesh refinement whereas the structured grid can not do so without introducing unnecessary unknows in regions with simple flow physics.

Typical results (velocity vector field, streamlines and pressure contours) are presented in Figure 11 for a case study. Process conditions for this case study are listed in the figure caption. In this example, both the static contact angle and the dynamic contact angle have been set to 145^o. Also, the downstream static contact line has been pinned (i.e. its location was fixed). As expected, pressure in the feed channel drops linearly. Two recirculations are present: a rather large and clearly visible one in the downstream region and a tiny one in

the upstream region that is not quite visible. It is informative that subambient pressure zones exist in both the upstream and downstream regions, in addition to that near the static and dynamic contact lines. Negative pressure is detrimental in coating flows because it can potentially cause cavitation of the coating liquid.

Figure 12 details a flow-field sequence when varying feed flowrate. As the feed flowrate was reduced from the initial 0.4 m/s to the final 0.07 m/s (Figure 12a), the mesh underwent very large deformation in the downstream region (the upstream free surface has been fixed in this parameter study). In all cases in the sequence, a mesh with the same topology was used. This sequence provides additional evidence of the robustness of our pseudo-solid mesh deformation technique. As shown in Figure 12b, no recirculation was present initially in the downstream region. When the feed flowrate was reduced to about 0.15 m/s or so, the downstream recirculation appeared and its size was enlarged as feed flowrate was further reduced.

Finally, Figure 13 shows the effects of varying vacuum applied at the upstream free surface. As expected, as vacuum was reduced, the upstream free surface moved inward toward the center (or the feed channel) but no visible changes were detected downstream (note that the scales for the three plots are slightly different; the slot gap height is the same for all three cases). Though not quite visible, the upstream recirculation shrank in size as vacuum was decreased.

4 Concluding Remarks

We have introduced two new features, namely unstructured grids and our novel pseudo-solid mesh deformation technique, in analyzing blade and slot coating flows, both of which have wide-spread applications in the paper-coating industry. We demonstrated the robustness and efficiency of our approach in limited case studies but its important implication to paper-coating-flow process design and optimization (via computer simulation) should be clear. We should also add that the work presented here reflects only the beginning of our effort at Sandia National Laboratories to develop a comprehensive software package that can be used for routine process design and optimization of coating processes such as blade and slot coating flows.

References

[1] D. F. Benjamin 1994 Roll Coating Flows and Multiple Roll Systems. *Ph.D. Thesis*, University of Minnesota, Minneapolis 55455.

[2] K. S. Chen 1992 Studies of Multilayer Slide Coating and Related Processes. *Ph.D. Thesis*, University of Minnesota, Minneapolis 55455.

[3] K. S. Chen and L. E. Scriven 1989 On the physics of liquid penetration into a deformable porous substrate. *1989 Coating Conference Proceedings*, TAPPI Press, Atlanta, pp.93-105.

[4] K. N. Christodoulou and L. E. Scriven. Discretization of free surface flows and other moving boundary problems. *Journal of Computational Physics*, 99:39–55, 1992.

[5] S. F. Kistler 1992 Hydrodynamics of wetting. In *Wettability*(Ed. J. C. Berg), Marcel Dekker, New York.

[6] S. F. Kistler and L. E. Scriven 1983 Coating flows. In *Computational Analysis of Polymer Processing*(Eds. J. R. Pearson and S. M. Richardson), Applied Science Publishers, London and New York.

[7] F. R. Pranckh and L. E. Scriven 1988 The physics of blade coating of deformable substrate. *1988 Coating Conference Proceedings*, TAPPI Press, Atlanta, pp.217-238.

[8] P. A. Sackinger, P. R. Schunk and R. R. Rao 1994 A finite element newton implementation of an implicit pseudo-solid domain mapping technique for free and moving boundary problems. Submitted to *J. of Comp. Phys.*

[9] L. Sartor 1990 Slot coating: fluid mechanics and die design. *Ph.D. Thesis*, University of Minnesota, Minneapolis 55455.

[10] P. R. Schunk 1989 Surfactant and polymer additives in coating and related flows. *Ph.D. Thesis*, University of Minnesota, Minneapolis 55455.

[11] A. B. Taylor 1978 Fluid flow between a roller and absorbent compressible paper. In *Quart. J. Mech. Appl. Math.*, **31**: 481-495 (1978).

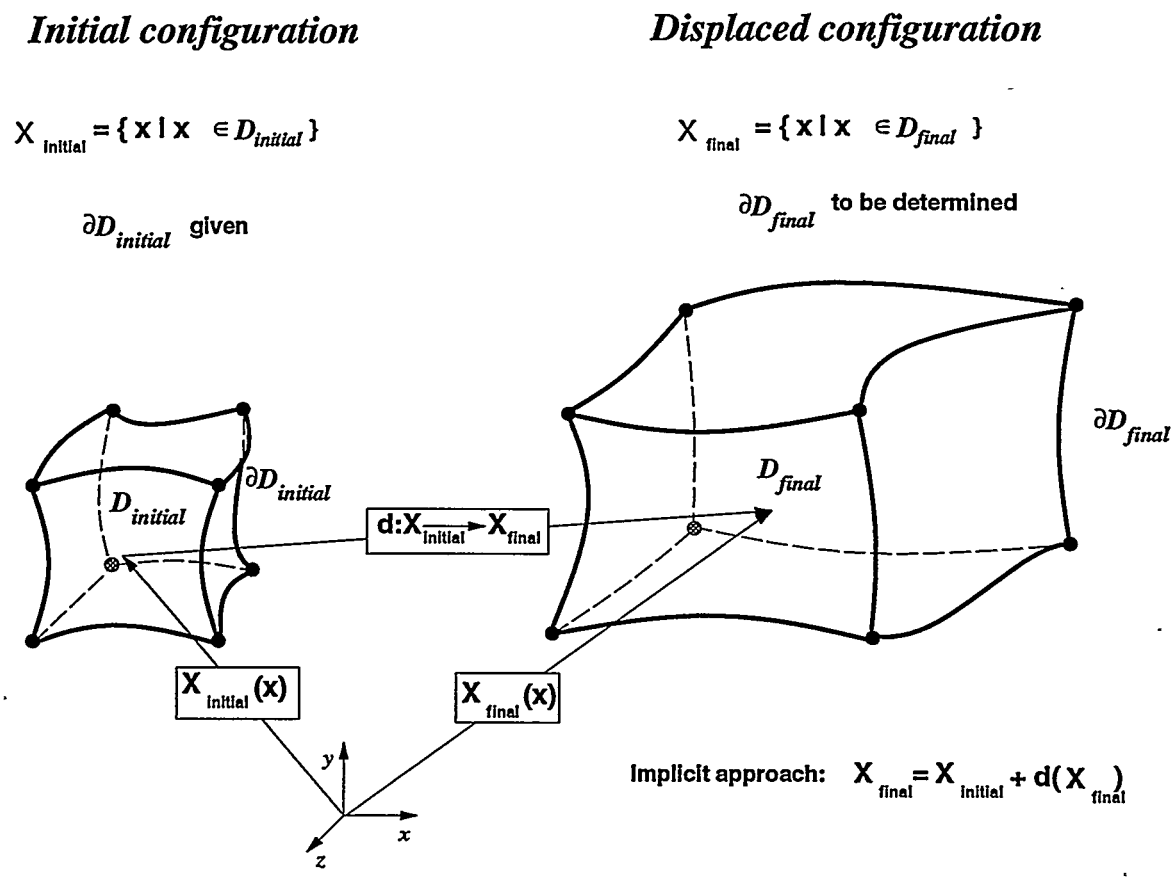

Figure 1: Mapping from the initial configuration to the final deform configuration.

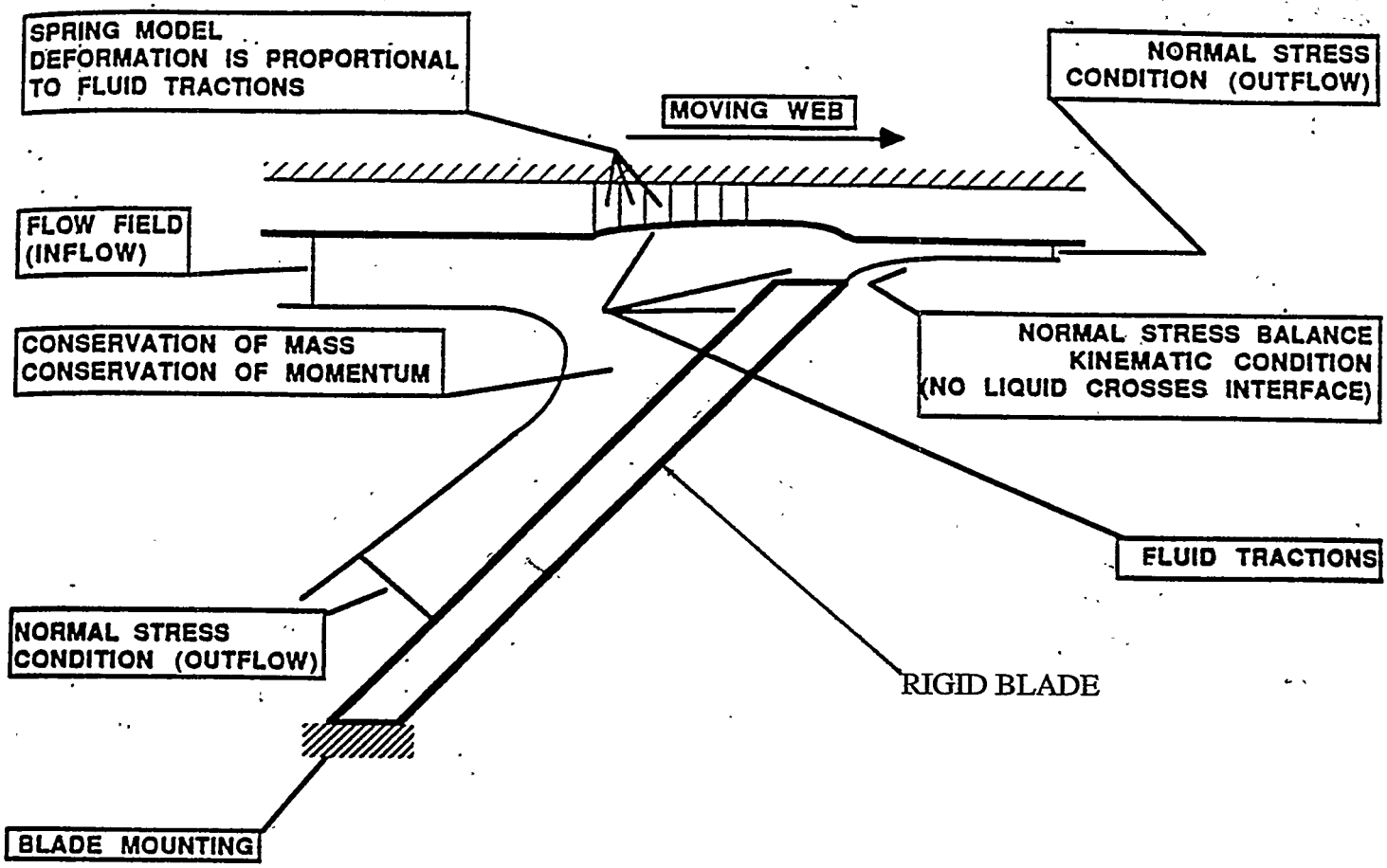

Figure 2. Blade Coating -- Governing principles and boundary conditions

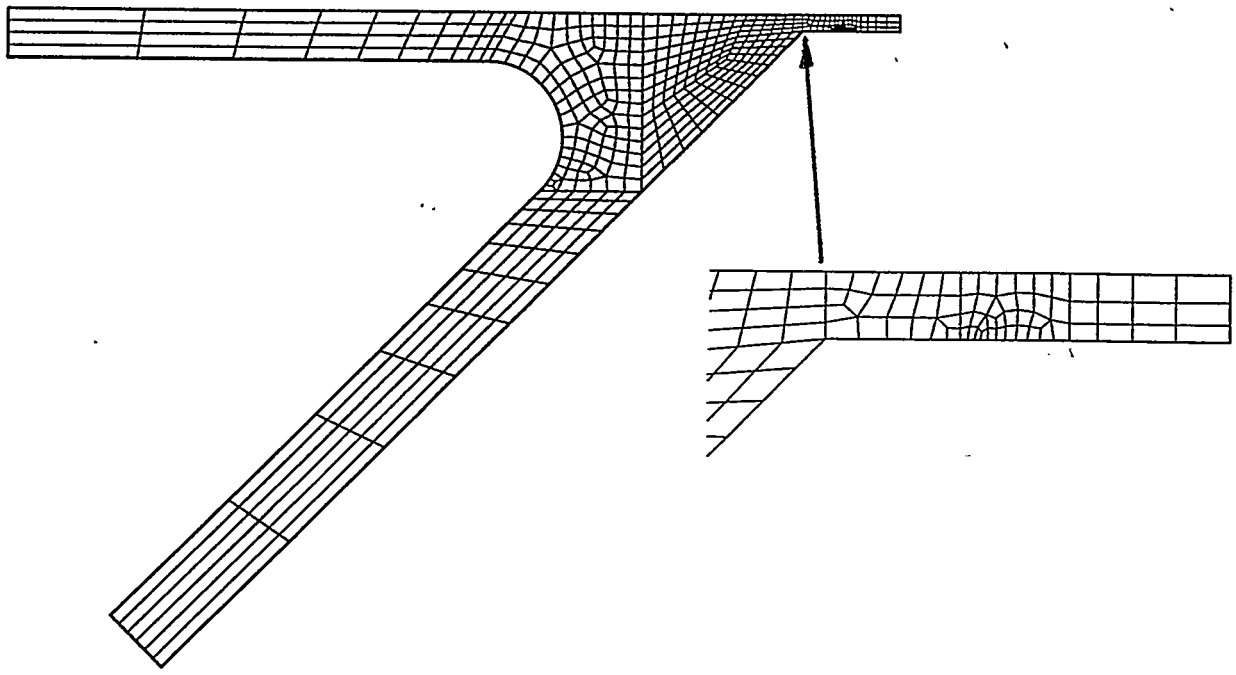

(a)

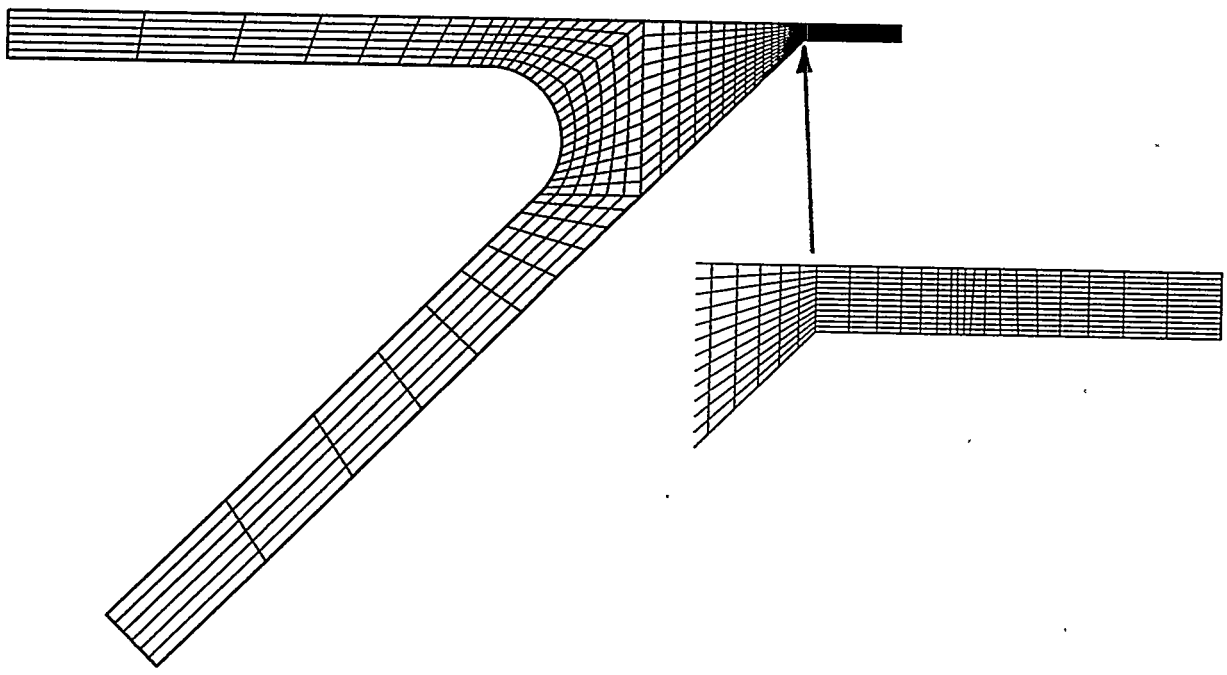

(b)

Figure 3. Finite Element Mesh Used in Blade Coating Flow Analysis
a). unstructured; b). structured.

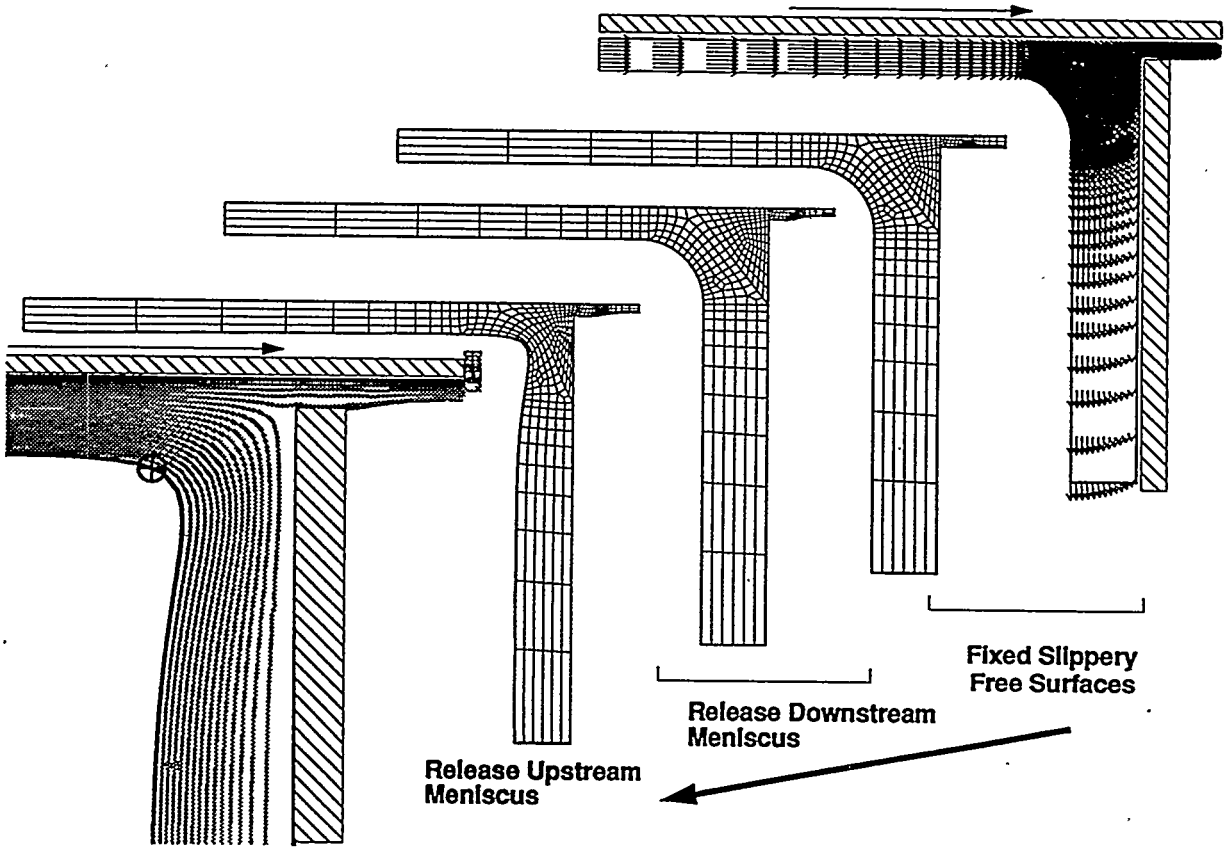

Figure 4. Blade Coating -- Startup Sequence

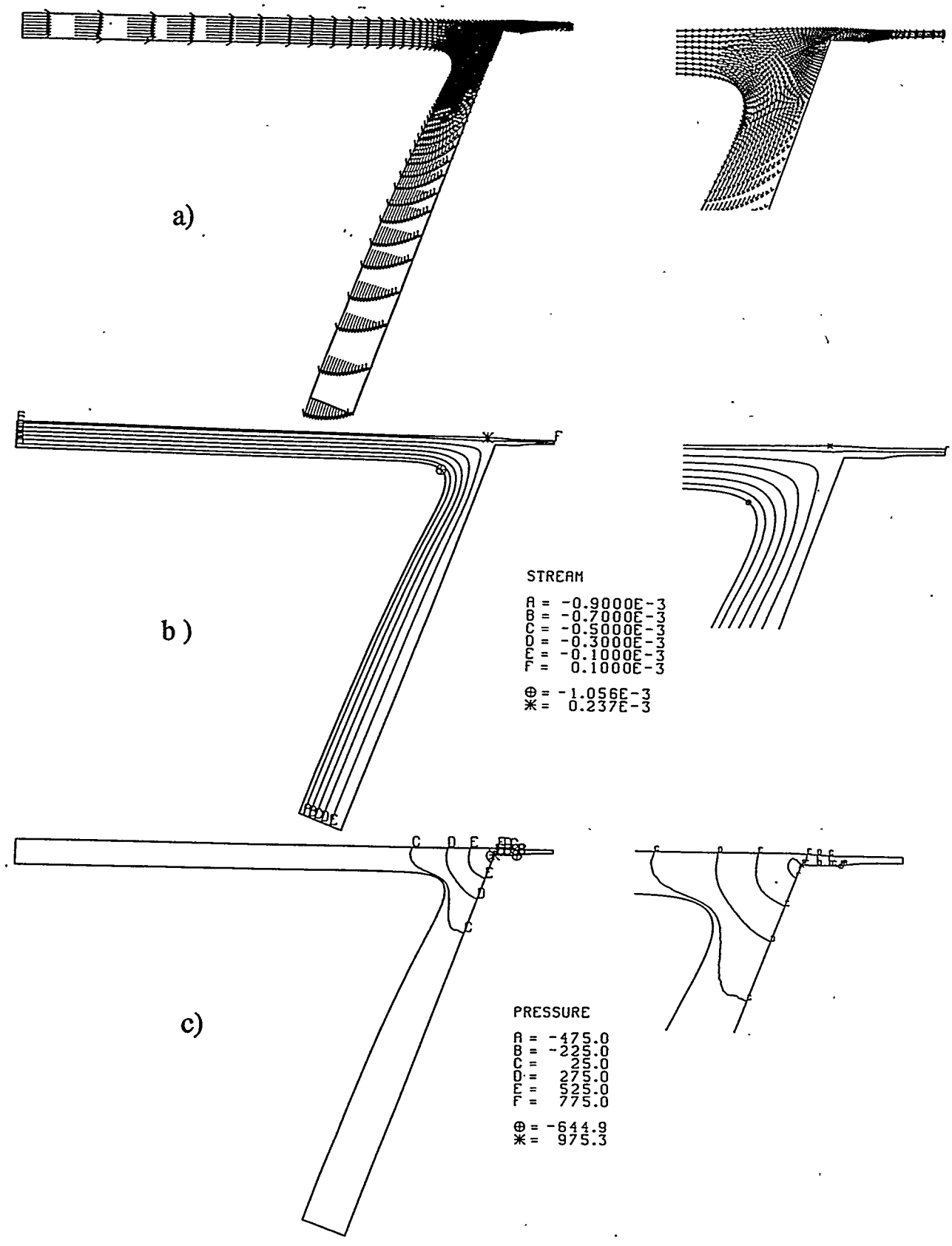

Figure 5. Blade Coating -- Typical Results
a). velocity field; b),streamlines; c). pressure control.

$(h_{IN} = 1.5mm, U_W = 1m/s, \rho = 1000kg/m^3, \mu = 50mPa \cdot s,$

$\sigma = 50mN/m, E = 5kPa, H_o = 0.3mm, \phi = 70^o)$

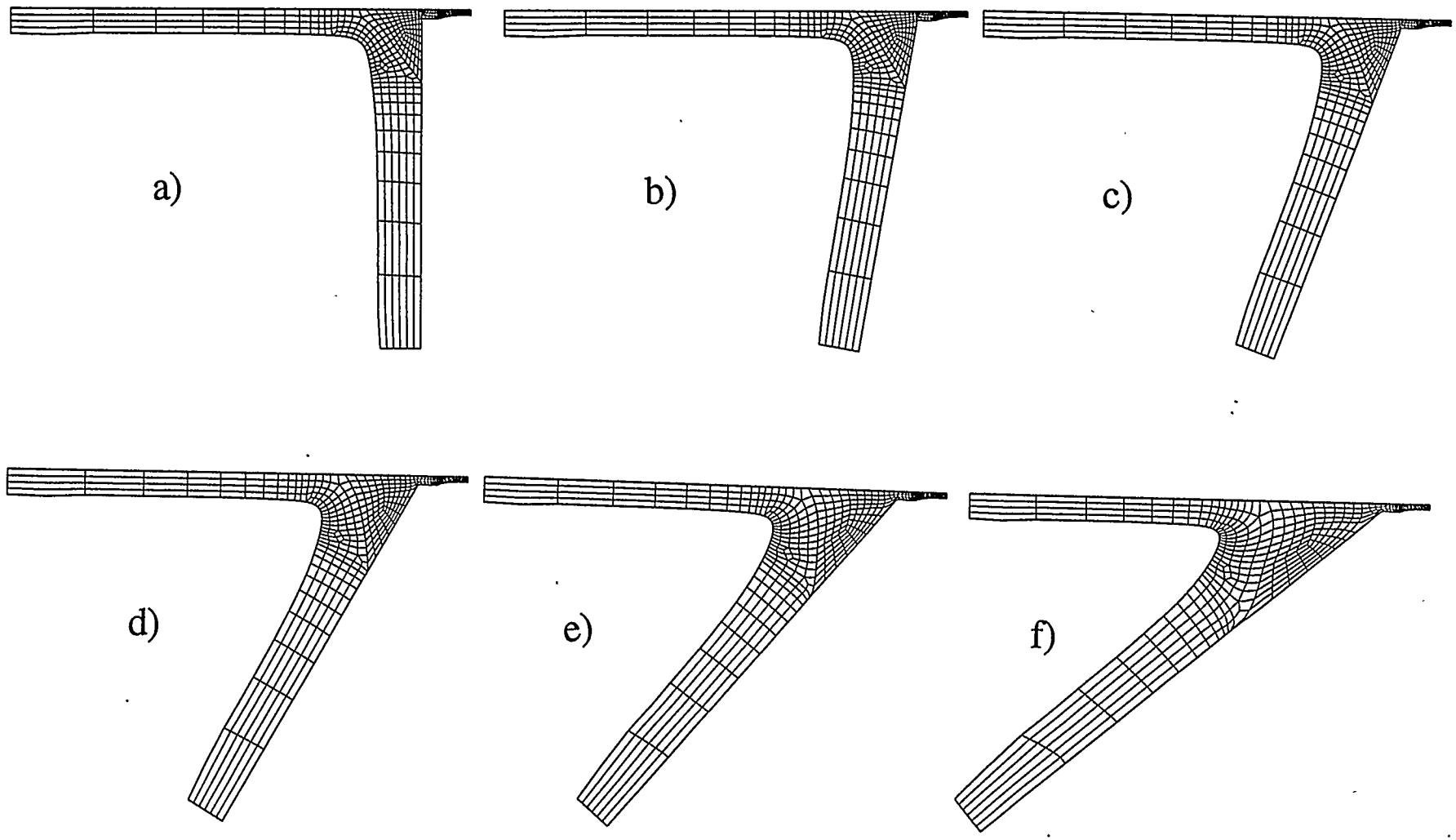

Figure 6a. Blade Coating -- Parameter Continuation in Blade Installation/Working Angle (mesh)
(without liquid inertia effects)

($h_{IN} = 1.5mm, U_W = 1m/s, \rho = 1000kg/m^3, \mu = 50mPa \cdot s, \sigma = 50mN/m, E = 50kPa, H_o = 0.3mm, \phi = 70^o$)

a). $\phi = 90^o$; b). $\phi = 80^o$; c). $\phi = 70^o$; d). $\phi = 60^o$; e). $\phi = 50^o$; f). $\phi = 40^o$.

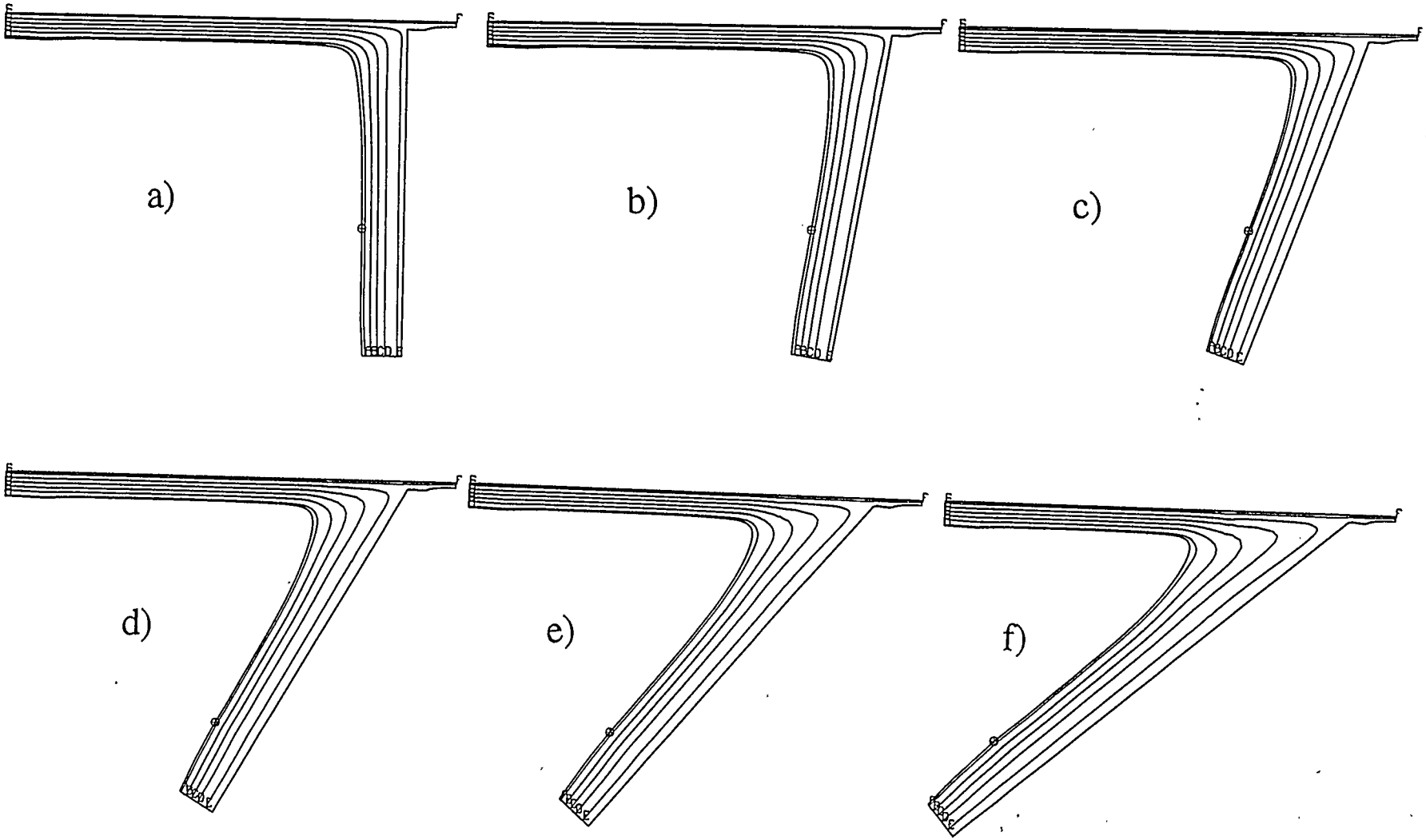

Figure 6b. Blade Coating -- Parameter Continuation in Blade Installation/Working Angle (streamlines)
(without liquid inertia effects)

($h_{IN} = 1.5mm, U_W = 1m/s, \rho = 1000kg/m^3, \mu = 50mPa \cdot s, \sigma = 50mN/m, E = 50kPa, H_o = 0.3mm, \phi = 70°$)

a). $\phi = 90°$; b). $\phi = 80°$; c). $\phi = 70°$; d). $\phi = 60°$; e). $\phi = 50°$; f). $\phi = 40°$.

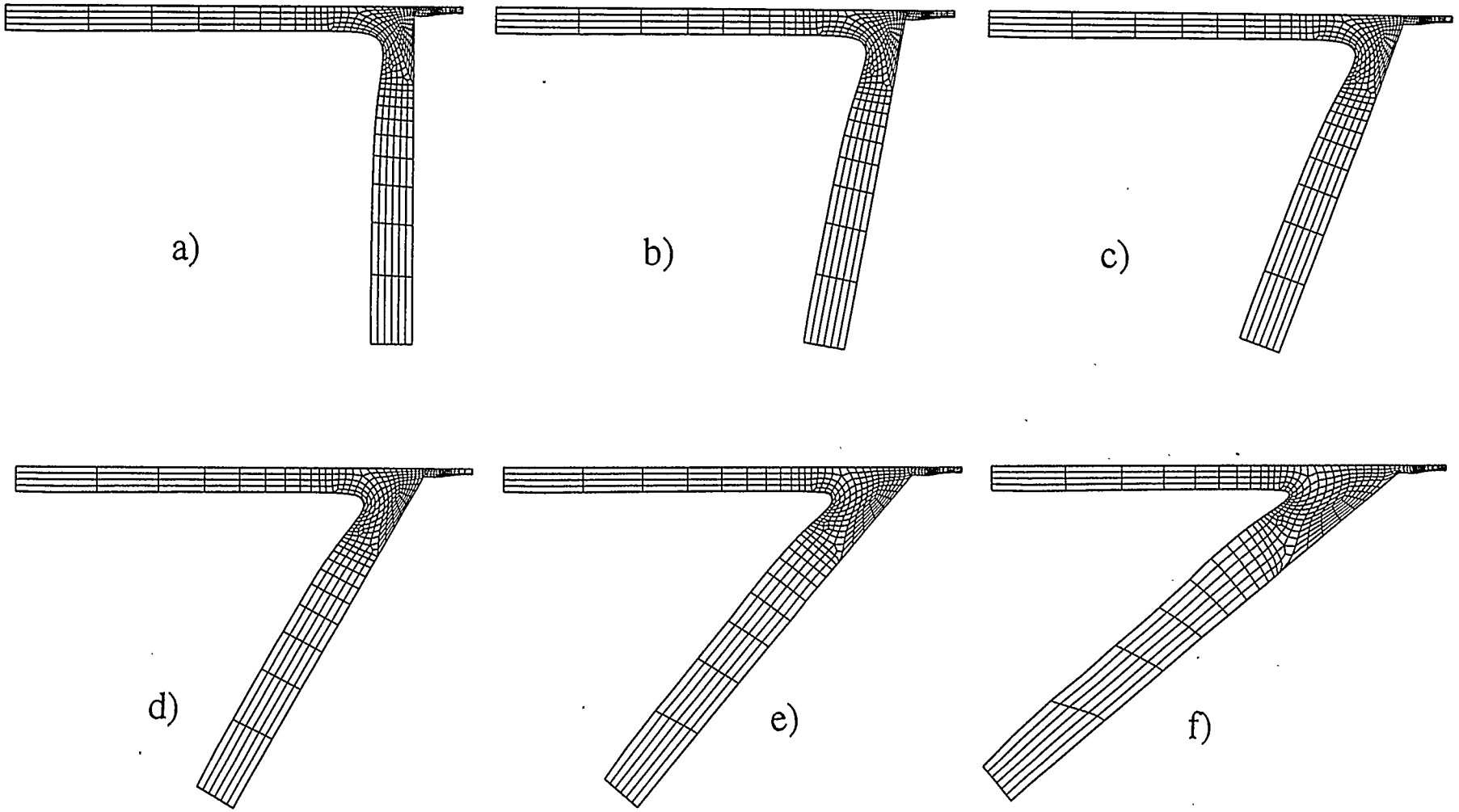

Figure 7a. Blade Coating — Parameter Continuation in Blade Installation/Working Angle(mesh; with liquid inertia effects)

$(h_{IN} = 1.5mm, U_W = 1m/s, \rho = 1000kg/m^3, \mu = 50mPa \cdot s, \sigma = 50mN/m, E = 50kPa, H_o = 0.3mm, \phi = 70°)$

a). $\phi = 90°$; b). $\phi = 80°$; c). $\phi = 70°$; d). $\phi = 60°$; e). $\phi = 50°$; f). $\phi = 40°$.

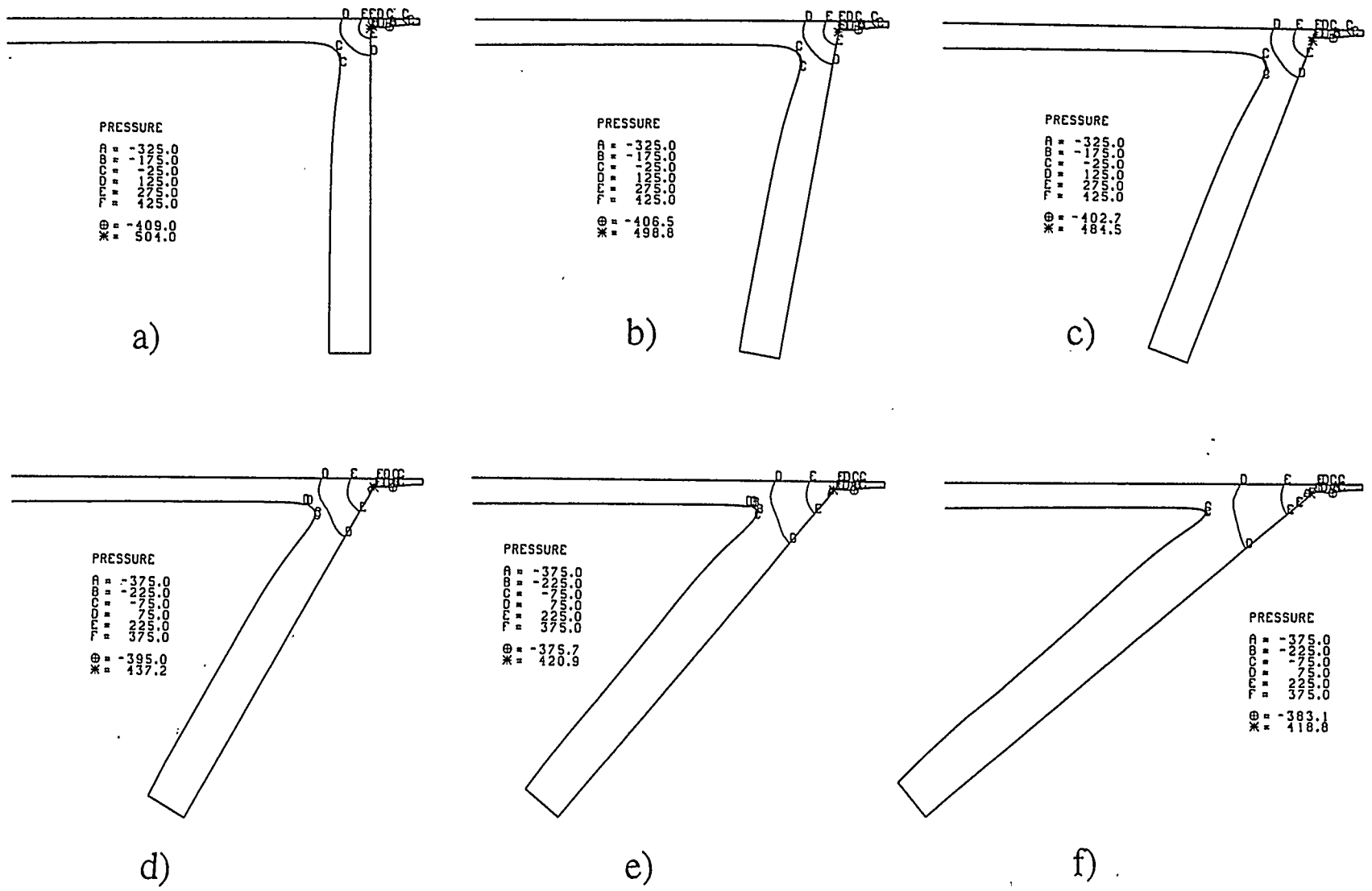

Figure 7b. Blade Coating — Parameter Continuation in Blade Installation/Working Angle(pressure contour; with liquid inertia effects)

$(h_{IN} = 1.5mm, U_W = 1m/s, \rho = 1000kg/m^3, \mu = 50mPa \cdot s, \sigma = 50mN/m, E = 50kPa, H_o = 0.3mm, \phi = 70°)$

a). $\phi = 90°$; b). $\phi = 80°$; c). $\phi = 70°$; d). $\phi = 60°$; e). $\phi = 50°$; f). $\phi = 40°$.

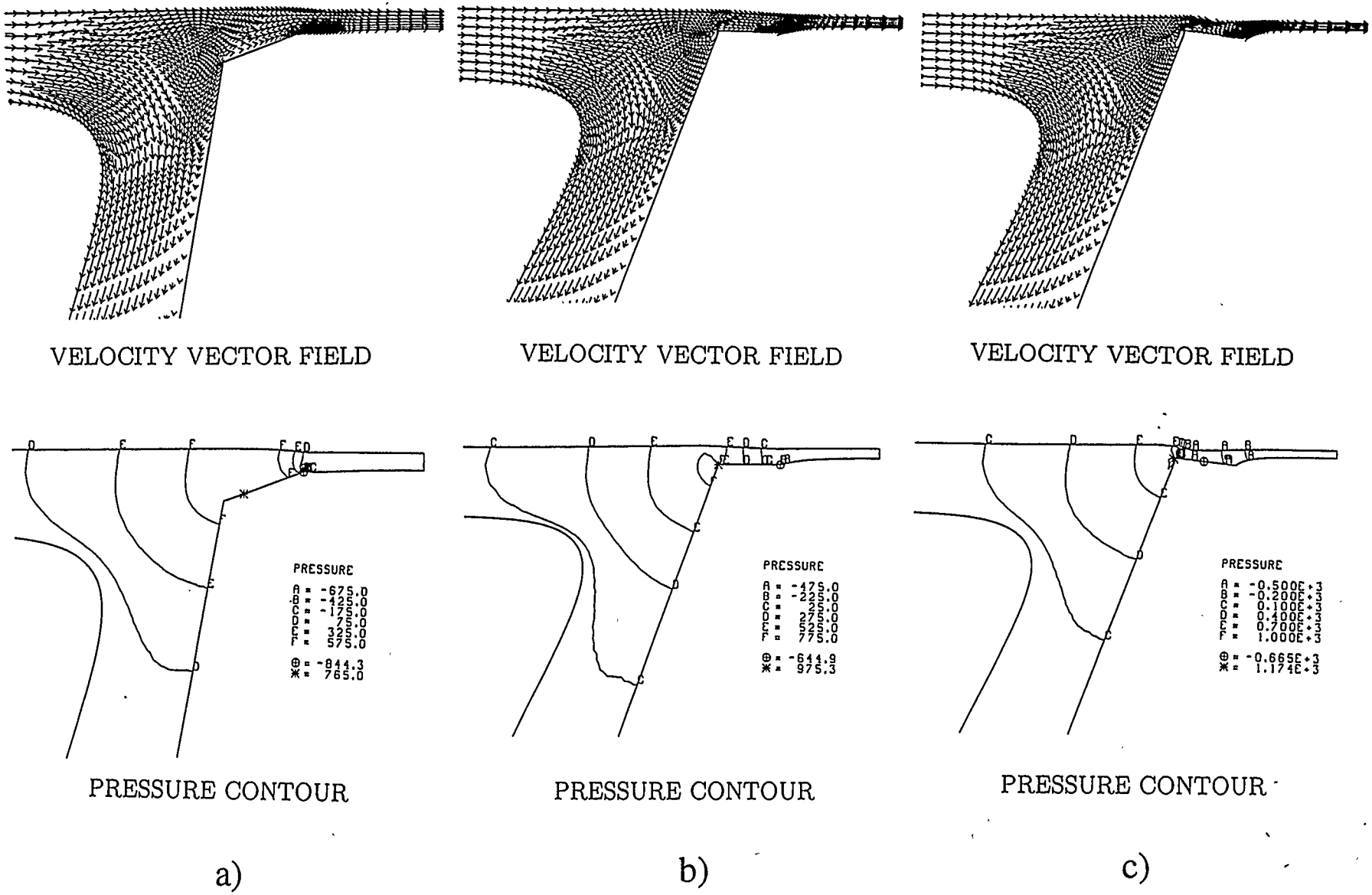

Figure 8. Blade Coating — Effects of Varying Blade Face Angle (θ)

a). $\theta = 20°$; b). $\theta = 0°$; c). $\theta = -6°$.

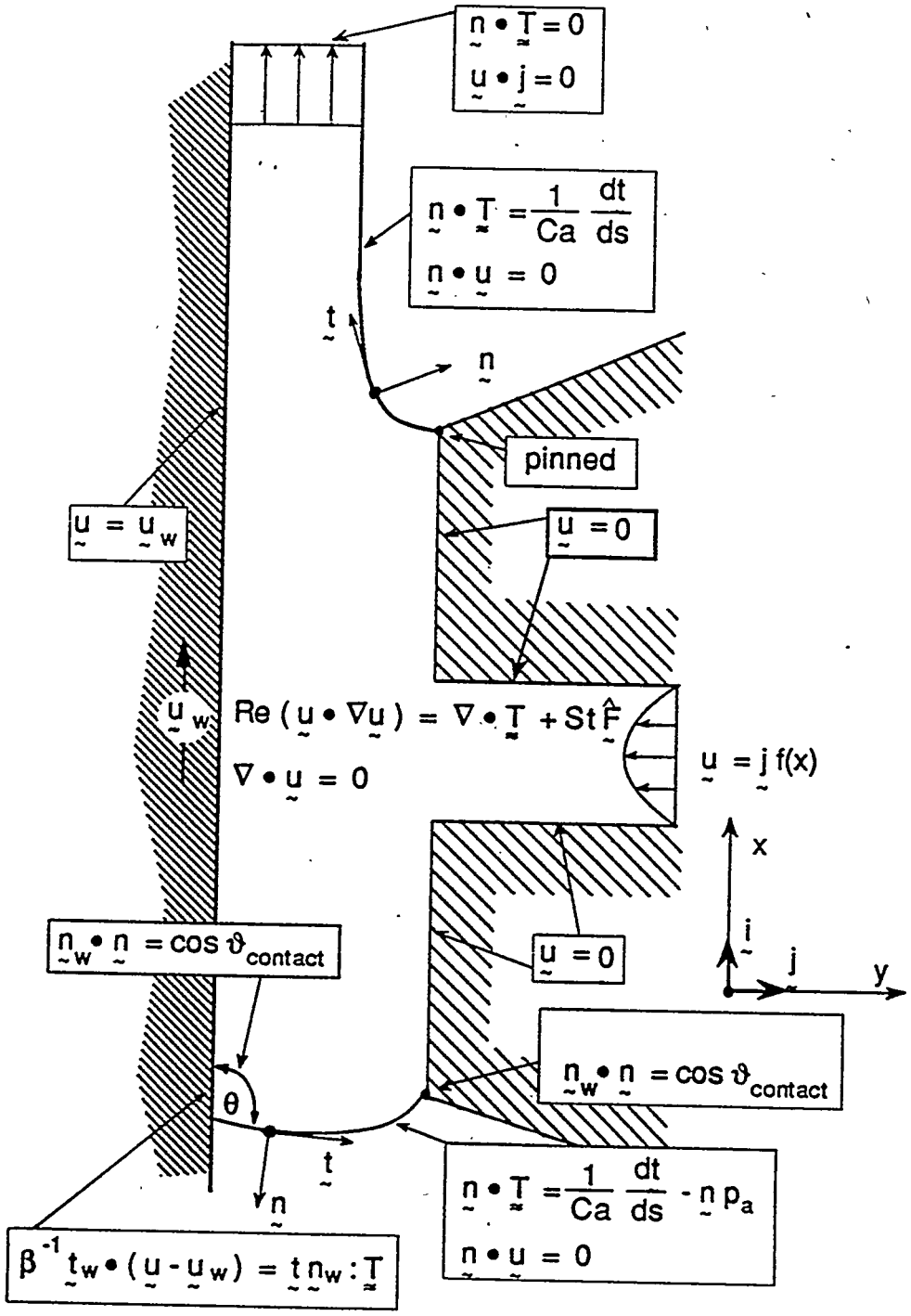

Figure 9. Slot Coating -- Governing principles and boundary conditions (Ref. Sartor 1990)

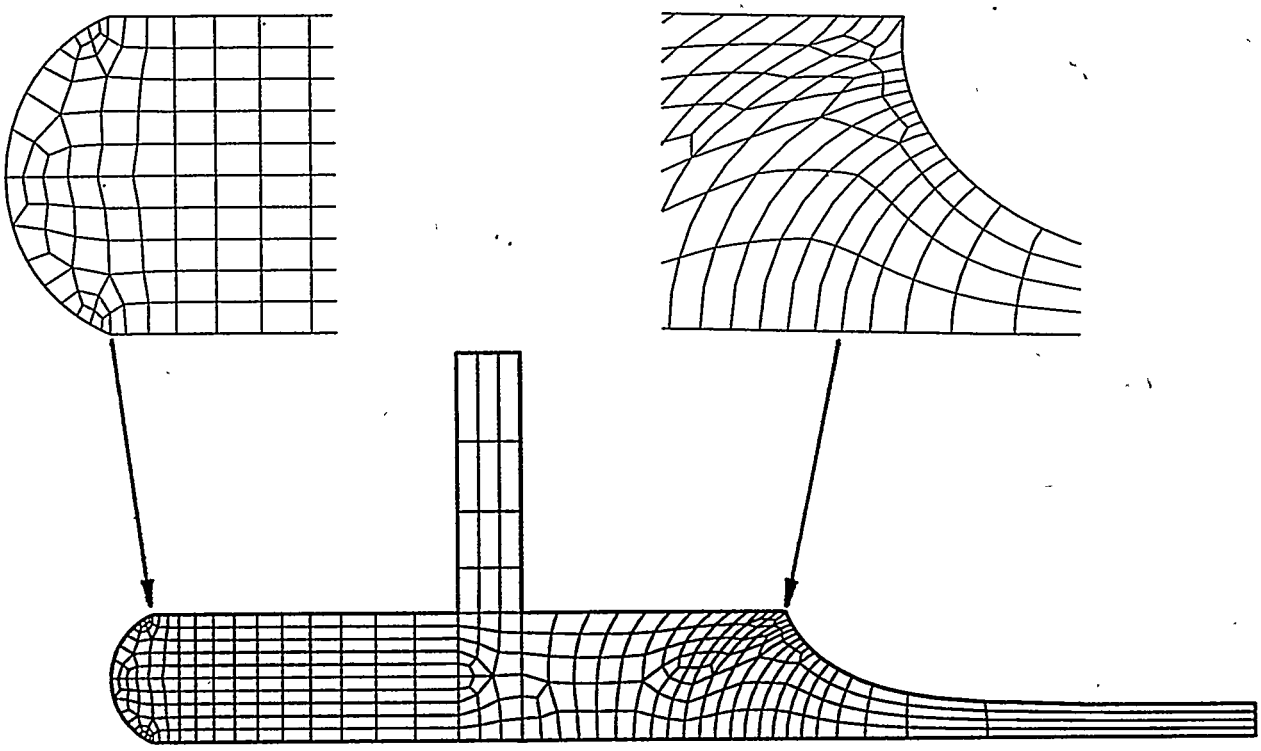

(a)

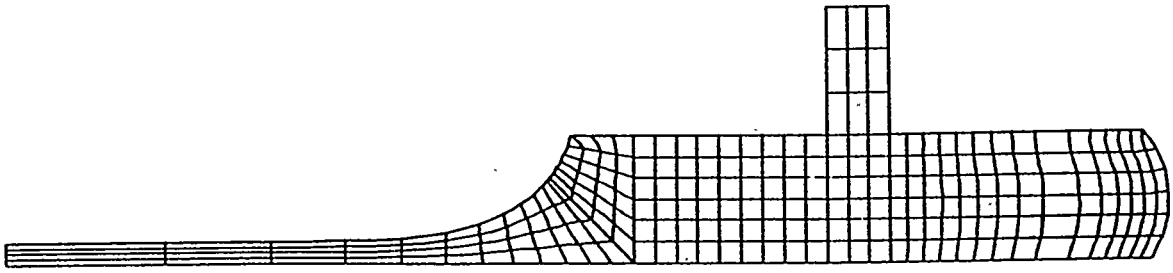

(b)

Figure 10. Finite Element Mesh Used in Slot Coating Flow Analysis
a). unstructured; b). structured (Sartor 1990).

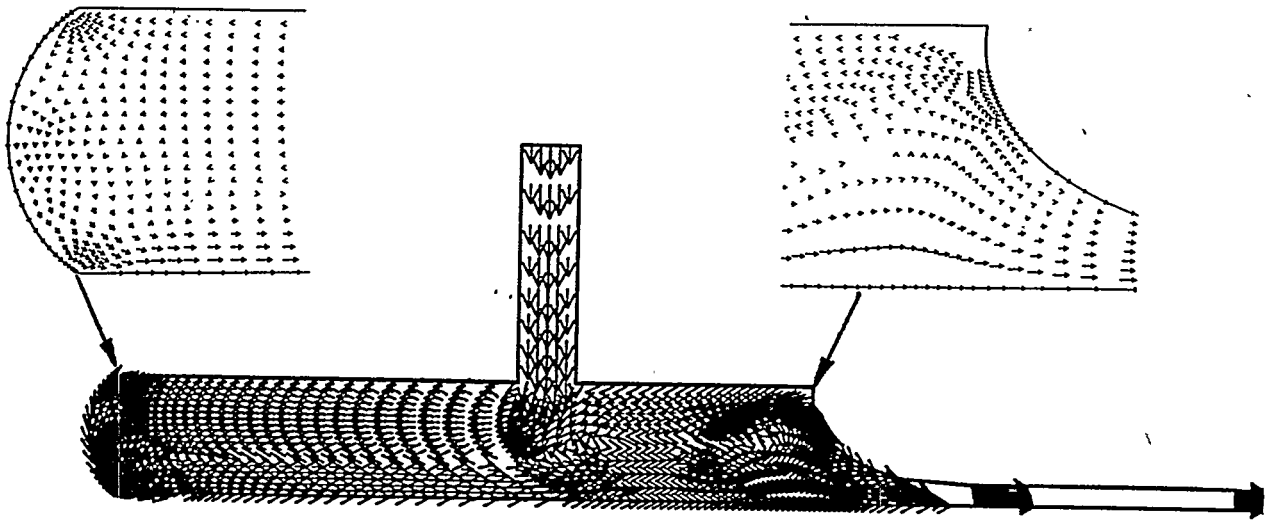

a)

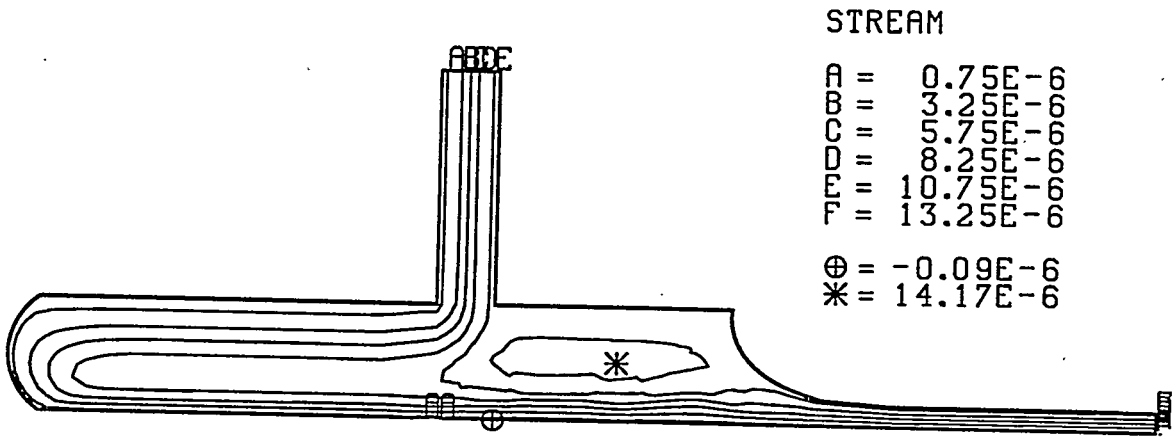

b)

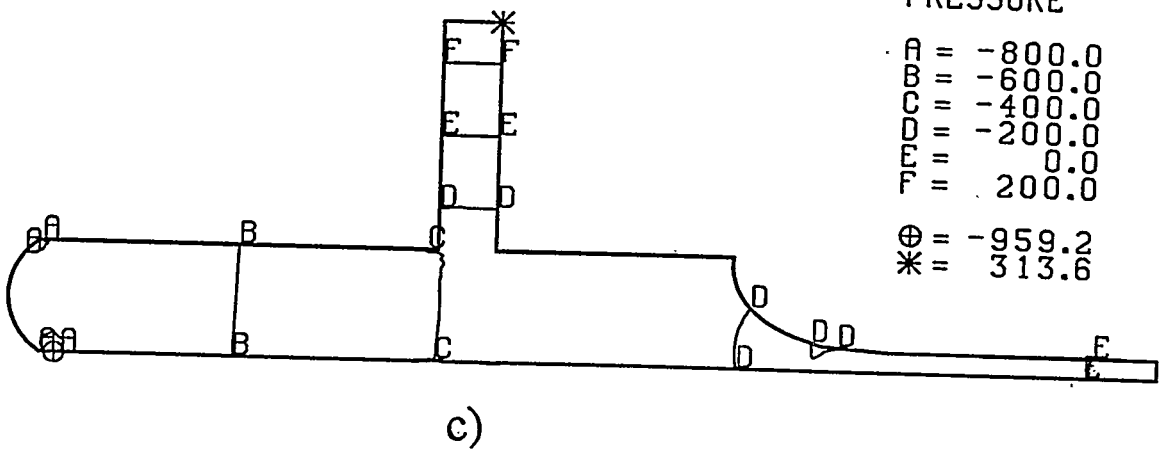

c)

Figure 11. Slot Coating — Typical results

($U_W = 0.133m/s$, $\rho = 1000kg/m^3$, $\mu = 70mPa \cdot s$, $\sigma = 65mN/m$, $\theta_s = 145^o$, $\theta_d = 145^o$, slot gap = 0.5mm). a). velocity vector field; b). streamlines; c). pressure contour.

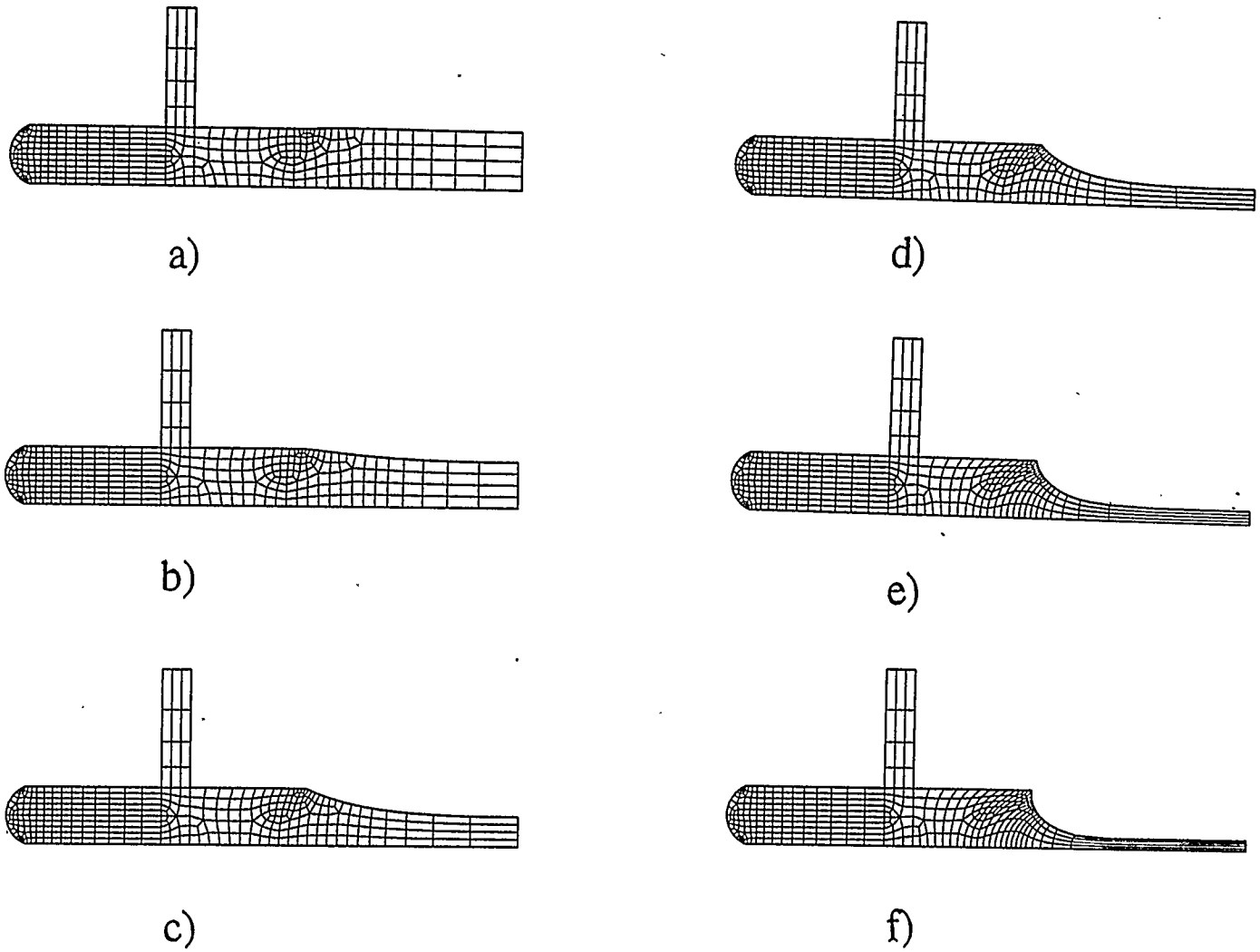

Figure 12a. Slot Coating — Parameter Continuation in Feed Flowrate (mesh)

($U_W = 0.133m/s$, $\rho = 1000kg/m^3$, $\mu = 70mPa \cdot s$, $\sigma = 65mN/m$, slot gap = 0.5mm; upstream free surface fixed).

a). Q = 0.4m/s; b). Q = 0.3m/s; c). Q = 0.2m/s; d). 0.133m/s; e). Q = 0.09m/s; f). Q = 0.07m/s.

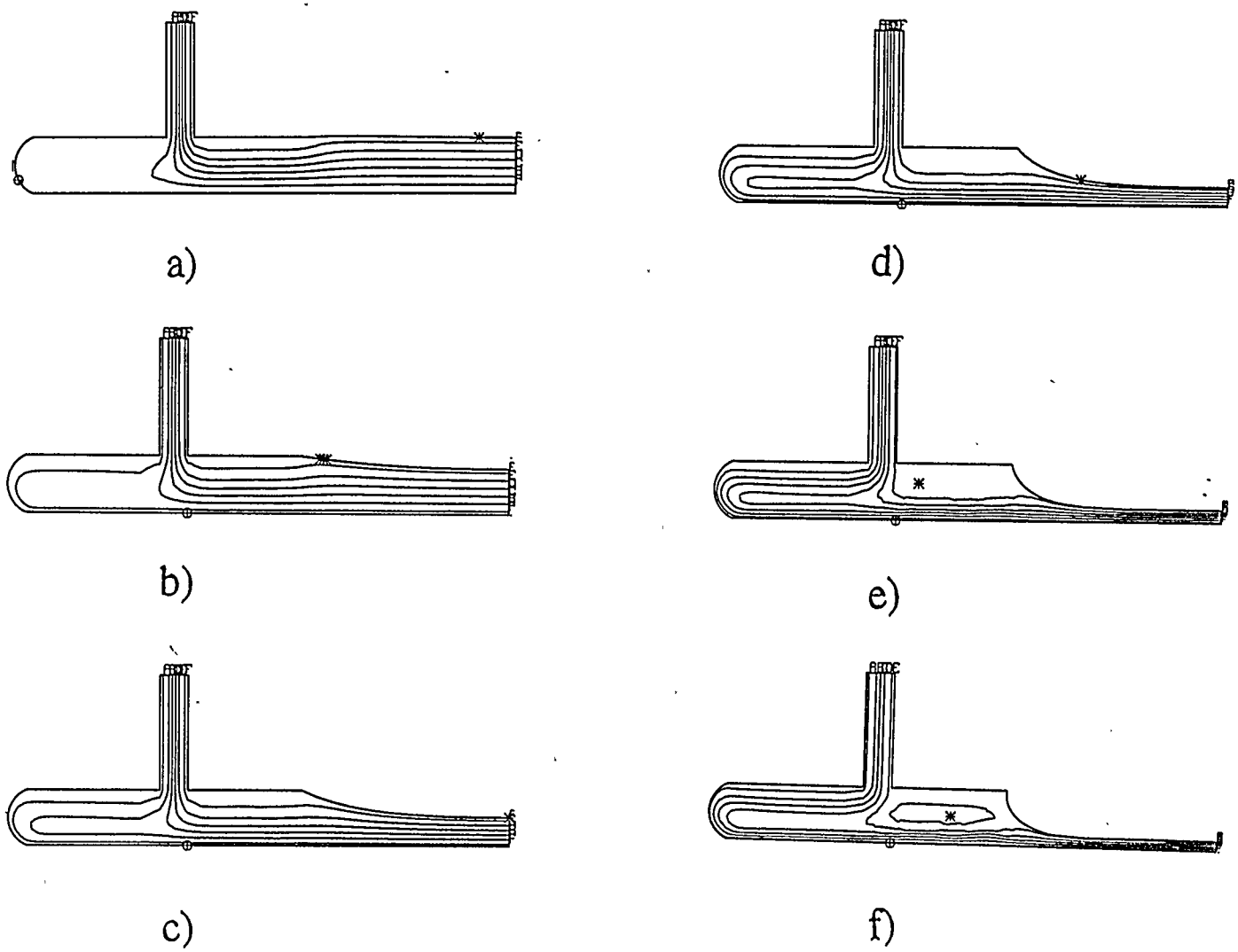

Figure 12b. Slot Coating — Parameter Continuation in Feed Flowrate (streamlines)

($U_W = 0.133m/s$, $\rho = 1000kg/m^3$, $\mu = 70mPa \cdot s$, $\sigma = 65mN/m$, slot gap = 0.5mm; upstream free surface fixed).

a). Q = 0.4m/s; b). Q = 0.3m/s; c). Q = 0.2m/s; d). 0.133m/s; e). Q = 0.09m/s; f). Q = 0.07m/s.

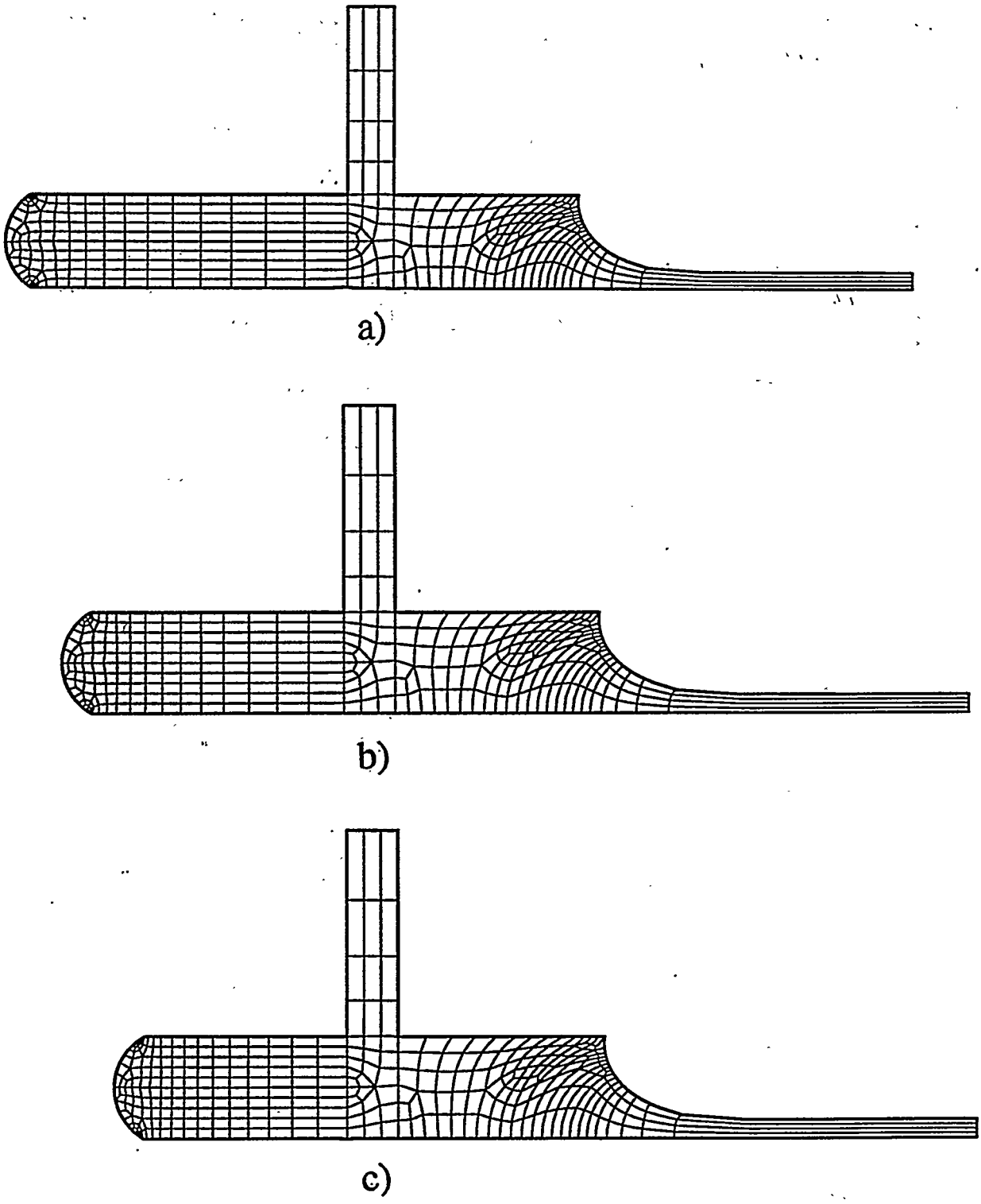

Figure 13a. Slot Coating — Effects of Vaccum (applied at Upstream Free Surface; mesh) ($U_W = 0.133m/s$, $\rho = 1000kg/m^3$, $\mu = 70mPa \cdot s$, $\sigma = 65mN/m$, slot gap = 0.5mm). a). $P_{VAC} = -1000Pa$; b). $P_{VAC} = -900Pa$; c). $P_{VAC} = -850Pa$.

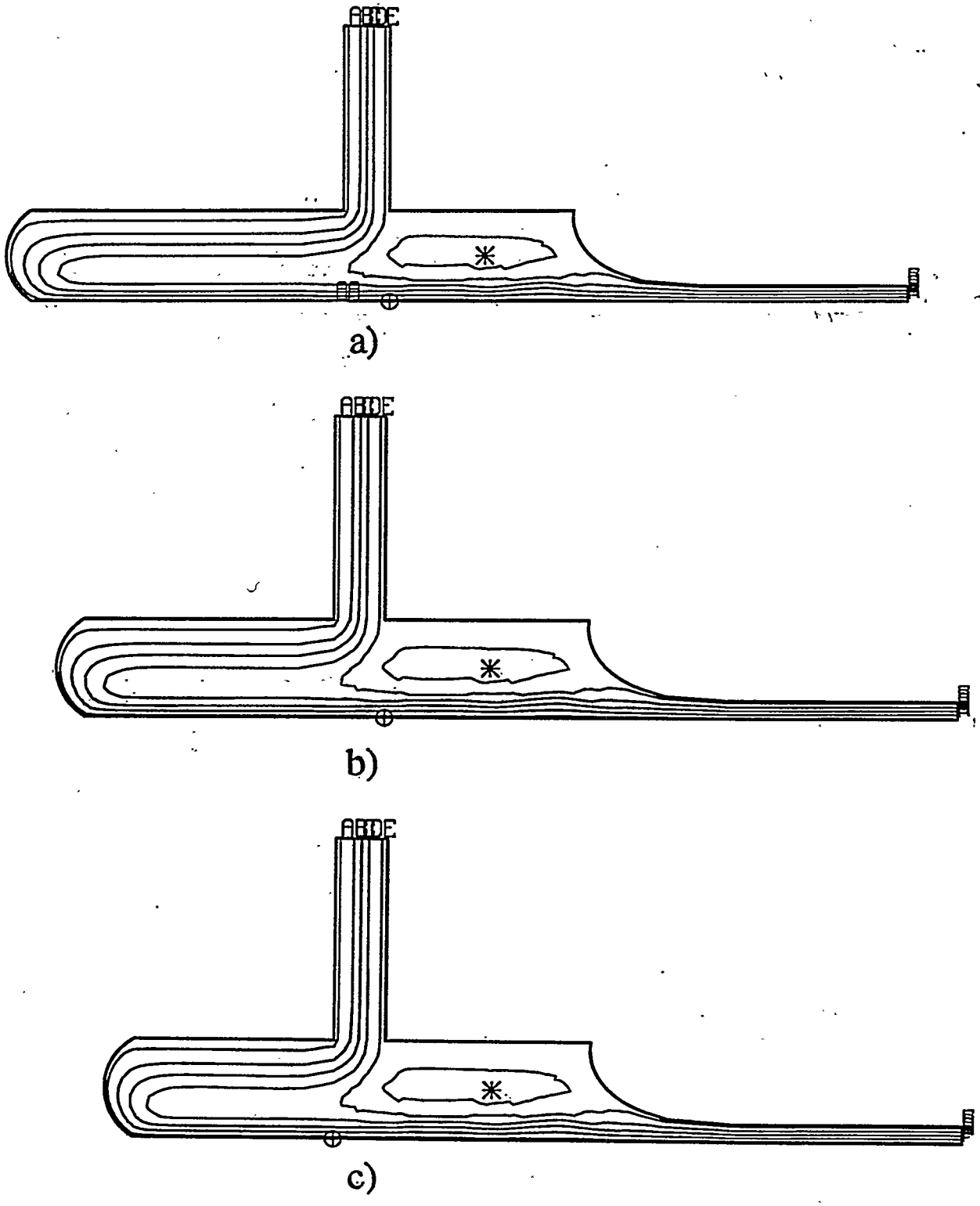

Figure 13b. Slot Coating — Effects of Vaccum (applied at Upstream Free Surface; streamlines) ($U_W = 0.133m/s$, $\rho = 1000kg/m^3$, $\mu = 70mPa \cdot s$, $\sigma = 65mN/m$, slot gap = 0.5mm). a). $P_{VAC} = -1000Pa$; b). $P_{VAC} = -900Pa$; c). $P_{VAC} = -850Pa$.